Determination of α_s in NNLO QCD using H1 jet cross section measurements

Vladimir Chekelian[1,⋆]

[1] *Max Planck Institute for Physics (Werner Heisenberg Institute), Munich*

Abstract. Measurements of jet cross sections in neutral current deep-inelastic scattering (NC DIS) using data taken with the H1 detector at HERA are accomplished by the precision measurement of double-differential inclusive jet, dijet and trijet cross sections at low photon virtualities $5.5 < Q^2 < 80$ GeV^2, and by extending previous inclusive jet measurements in the range $150 < Q^2 < 15000$ GeV^2 to low transverse jet momenta $5 < P_T < 7$ GeV. The strong coupling constant at the Z-boson mass, $\alpha_s(m_Z)$, is determined in next-to-next-to-leading order (NNLO) QCD using H1 inclusive jet and dijet cross section measurements. Complementary, $\alpha_s(m_Z)$ is determined together with parton distribution functions of the proton (PDFs) from jet and inclusive DIS data measured by the H1 experiment. The running of the strong coupling is tested at different values of the renormalisation scale and the results are found to be in agreement with the QCD expectations.

1 Introduction

Jet production in neutral current deep-inelastic scattering (NC DIS) at HERA is an important process to test perturbative calculations based on Quantum Chromodynamics (QCD), the theory of strong interactions. In the Breit frame, where the virtual photon and the proton collide head on, the jet production process always involves at least one strong vertex and, therefore, is well suited for a determination of the strong coupling α_s.

The jet measurements program in NC DIS at HERA by the H1 collaboration is now completed, see [1] and references in [2]. The last piece of this scientific program [1], an extension of the measured range to low negative four-momentum transfer squared, $5.5 < Q^2 < 80\,\text{GeV}^2$, and, for previous inclusive jet measurements in the range $150 < Q^2 < 15000$ GeV^2 [3], to low transverse jet momenta $5 < P_T < 7$ GeV, is presented here together with the first determination [2] of the strong coupling constant at the Z-boson mass, $\alpha_s(m_Z)$, which is making use of recent calculations of jet production at next-to-next-to-leading order in QCD (NNLO) [4–7], applied to the H1 jet data. These NNLO calculations are also used for the first time for the determination of parton distribution functions of the proton (PDFs).

⋆On behalf of the H1 Collaboration

2 Jet production measurements at low Q^2

For the low-Q^2 analysis [1] the data sample was collected with the H1 detector at HERA in the years 2005 to 2007, where electron or positron[1] beams with an energy of $E_e = 27.6\,\text{GeV}$ collided with protons of energy $E_p = 920\,\text{GeV}$, resulting in a centre-of-mass energy of $\sqrt{s} = 319\,\text{GeV}$. The integrated luminosity corresponds to $290\,\text{pb}^{-1}$. Double-differential cross sections of inclusive jet, dijet and trijet cross sections are obtained, extending the kinematic range of an earlier measurement both to lower momentum transfer, $5.5 < Q^2 < 80\,\text{GeV}^2$, and to lower jet transverse momenta. The transverse momenta of jets in the Breit frame, P_T^jet, are required to exceed 4 GeV . Inclusive jet cross sections are measured in the jet transverse momenta range $4.5 < P_\text{T}^\text{jet} < 50\,\text{GeV}$. Dijet cross sections are measured as a function of the average transverse momentum of the two jets with the highest P_T^jet in an event, $\langle P_\text{T}\rangle_2 = \frac{1}{2}(P_\text{T}^\text{jet1} + P_\text{T}^\text{jet2})$, in the range $5 < \langle P_\text{T}\rangle_2 < 50\,\text{GeV}$, and trijet cross sections as a function of $\langle P_\text{T}\rangle_3 = \frac{1}{3}(P_\text{T}^\text{jet1} + P_\text{T}^\text{jet2} + P_\text{T}^\text{jet3})$ in the range $5.5 < \langle P_\text{T}\rangle_3 < 40\,\text{GeV}$. At large momentum transfer, $150 < Q^2 < 15\,000\,\text{GeV}^2$, an extension of previously published inclusive jet cross section measurements to lower transverse jet momenta, $5 < P_\text{T}^\text{jet} < 7\,\text{GeV}$, is presented.

The measured jet data are corrected for effects of detector acceptance, efficiency and resolution using a regularised unfolding [8]. A detector response matrix with elements a_{ij} expressing the probability for an observable originating in the generated MC sample from an interval i to be measured in an interval j, is determined using the average of the reweighted Djangoh [9] and Rapgap [10] MC simulations. Migrations from the 'extended analysis phase space' to the 'measurement phase space', are included via additional rows and columns in the detector response matrix. The resulting migration matrix, which takes into account statistical correlations between NC DIS, inclusive jets, dijet and trijet measurements, has a size of 3381 (on the hadron level) times 12 300 (on the detector level) elements. For the final cross sections on the hadron level, 320 unfolded values are used. For the final inclusive jet cross sections, 168 unfolded values are used to calculate the 48 data points. Respectively, 88 and 56 unfolded values are used to obtain the 48 dijet and 32 trijet data points.

The jet cross sections obtained are hadron level cross sections corrected for radiative QED effects. The cross section data point k is calculated as

$$\sigma_k = c_k^\text{rad} \frac{n_k^\text{unfolded}}{\mathcal{L}}\,, \tag{1}$$

where n_k^unfolded is the sum of the unfolded numbers of events in bins corresponding to the data point k, c_k^rad denotes the correction for QED radiative effects, and $\mathcal{L}$ is an integrated luminosity.

The simultaneous unfolding of the inclusive NC DIS measurement together with the jet measurements, respecting all statistical correlations, allows for the determination of jet cross sections normalised to the inclusive NC DIS cross section. Normalised jet cross sections are defined as the ratio of the double-differential absolute jet cross section to the NC DIS cross section in the respective Q^2-bin k_q:

$$\sigma_k^\text{norm} = \frac{\sigma_k}{\sigma_{k_q}^\text{NC}} \tag{2}$$

Double-differential cross sections of the inclusive jet, dijet and trijets production are measured [1] as a function of P_T^jet , $\langle P_\text{T}\rangle_2$ or $\langle P_\text{T}\rangle_3$ at different values of Q^2 .

Ratios of the inclusive jet cross section measurements to the NLO predictions are shown in figure 1. The bin at low P_T^jet for $150 < Q^2 < 15000\,\text{GeV}^2$ corresponds to the extension of the high-Q^2

[1] The term 'electron' is used in the following to refer to both electron and positron.

measurements [3] to the region $5 < P_T^{jet} < 7$ GeV [1]. The ratios are compared with the similar theory ratios of the theoretical predictions in NNLO [4–7] and in approximate NNLO corresponding to NLO supplemented with two-loop threshold corrections (aNNLO) [11, 12]. In general, the data are well described by the predictions within experimental and theoretical uncertainties. The central values of the NLO and the aNNLO predictions are lower than the data in most bins, while the NNLO predictions have a tendency to lie above the data. At lower values of Q^2, NLO predicts harder P_T^{jet}-spectra than observed. The NNLO predictions give a good description of the P_T^{jet}-distributions. The aNNLO predictions provide a reasonable description of the shape of the P_T^{jet}-distributions.

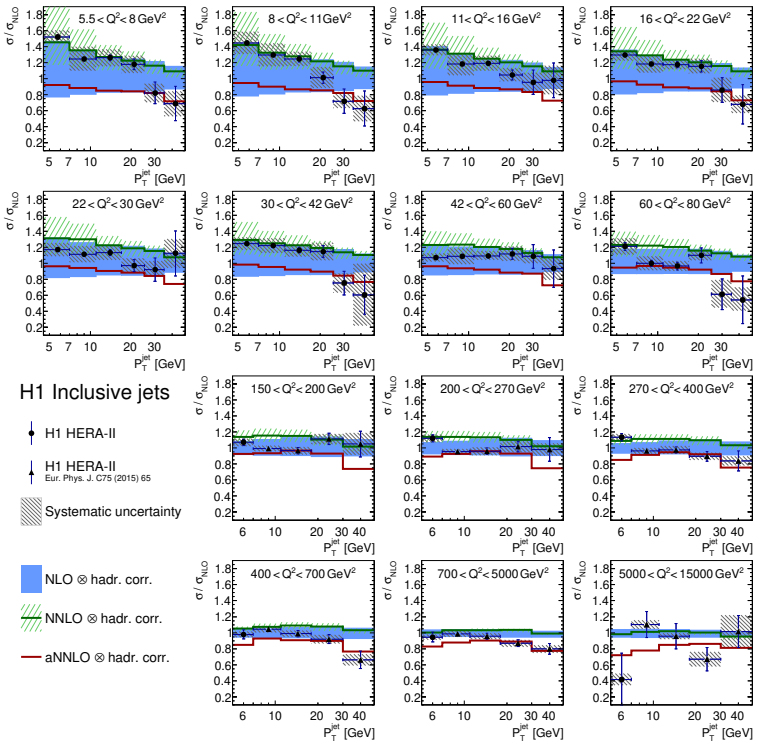

Figure 1. Ratio of inclusive jet cross section measurements to the NLO predictions as a function of Q^2 and P_T^{jet}. The new data are presented as full circles. The NNLO and aNNLO predictions are also shown.

A comparison of the ratio of the double-differential dijet cross sections to NLO predictions with the predictions in NNLO and in aNNLO is shown in figure 2 (left) as a function of $\langle P_T \rangle_2$ and Q^2. Within the scale uncertainties, the data are described well by the QCD predictions. However, the NNLO and aNNLO predictions provide a better description of the shapes than the NLO predictions.

The ratio of the double-differential trijet cross sections to NLO predictions as function of $\langle P_T \rangle_3$ and Q^2 is displayed in figure 2 (right). The NLO calculations give an overall good agreement with the data over the full phase space. However, a trend to undershoot the data at lower values of $\langle P_T \rangle_3$ and to overshoot them at higher values of $\langle P_T \rangle_3$ is observed, which is more pronounced at lower values of Q^2.

In order to obtain the normalised inclusive jet, dijet and trijet cross sections as defined in equation 2, cross sections for inclusive NC DIS are measured in the Q^2 bins for $0.2 < y < 0.6$. The relative

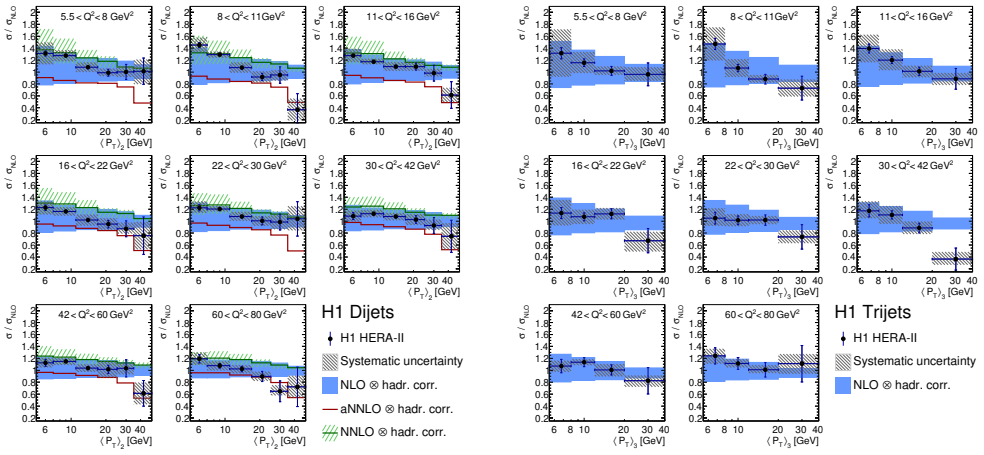

Figure 2. Ratio of dijet (left) and trijet (right) cross section measurements to the NLO predictions as a function of Q^2 and $\langle P_{\mathrm{T}} \rangle_2$ or $\langle P_{\mathrm{T}} \rangle_3$. For dijets the NNLO and aNNLO prediction are also shown.

experimental uncertainties of the normalised jet cross sections are of similar size as the ones of the absolute jet cross sections.

3 Determination of $\alpha_{\mathrm{s}}(m_{\mathrm{Z}})$ from H1 jet cross sections

The strong coupling constant $\alpha_{\mathrm{s}}(m_{\mathrm{Z}})$ is determined [2] from inclusive jet and dijet cross sections in NC DIS measured by the H1 collaboration using recent NNLO QCD calculations [4–7].

Cross sections for jet production have been measured by H1 at two different centre-of-mass energies using data from different periods of data taking. Inclusive jet and dijet cross sections measured in the range $5 < Q^2 < 15\,000\,\mathrm{GeV}^2$ and inelasticities $0.2 < y < 0.7$ are considered. Common to all data, jets are defined in the Breit frame using the k_t clustering algorithm with a resolution parameter $R = 1$. The jet four-vectors are restricted to the pseudorapidity range $-1 < \eta^{\mathrm{jet}}_{\mathrm{lab}} < 2.5$ in the laboratory frame. The data sets '300 GeV', 'HERA-I' and 'HERA-II' correspond to different data taking periods and are subdivided into two kinematic ranges, the low-Q^2 ($Q^2 \lesssim 100\,\mathrm{GeV}^2$) and high-$Q^2$ ($Q^2 \gtrsim 150\,\mathrm{GeV}^2$) domains, where different components of the H1 detector were used for the measurement of the scattered lepton. In total 9 data sets of inclusive jet and dijet cross sections measured double-differentially as functions of Q^2 and the jet transverse momentum are used.

In order to avoid regions of phase space where the predictions exhibit an enhanced infrared sensitivity, the phase space definitions impose asymmetric cuts on the transverse momenta of the two leading jets. Such an asymmetric cut may also be obtained by choosing $\langle P_{\mathrm{T}} \rangle$ larger than the minimum $P^{\mathrm{jet}}_{\mathrm{T}}$. For this reason, data points with $\langle P_{\mathrm{T}} \rangle < 7\,\mathrm{GeV}$ are excluded from the HERA-I low-Q^2 data set.

The renormalisation μ_{R} and factorisation μ_{F} scales in this analysis are chosen to be

$$\mu^2_{\mathrm{R}} = \mu^2_{\mathrm{F}} = Q^2 + P^2_T \,, \tag{3}$$

where P_T denotes $P^{\mathrm{jet}}_{\mathrm{T}}$ in the case of inclusive jet cross sections and $\langle P_{\mathrm{T}} \rangle_2$ for dijets.

The ratios of inclusive jet and dijet cross sections to NNLO predictions are shown in figure 3 as a function of the scale value of the data point $\tilde{\mu}$.

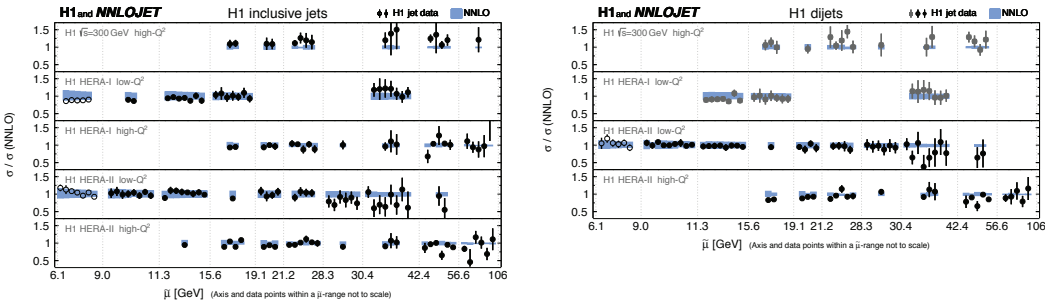

Figure 3. Ratio of inclusive jet (left figure) and dijet cross sections (right figure) to NNLO predictions obtained with the fitted value $\alpha_s(m_Z) = 0.1157$. Data points are displayed on the horizontal axis within the respective $\tilde{\mu}$-intervals with equal horizontal spacing and are thus not to scale. The open circles show data points which are not considered for some fits, because their scale $\tilde{\mu}$ is below two masses of the b-quark.

Theory

The cross sections for inclusive jet and dijet production for a given phase space interval i are calculated as a convolution in the variable x of the PDFs f_k and perturbatively calculated partonic cross sections $\hat{\sigma}_{i,k}$,

$$\sigma_i = \sum_{k=g,q,\bar{q}} \int dx f_k(x,\mu_F) \hat{\sigma}_{i,k}(x,\mu_R,\mu_F) \cdot c_{had,i} \,, \tag{4}$$

where the sum runs over all parton flavours k. The calculations depend on the scales μ_R and μ_F. The factors $c_{had,i}$ account for non-perturbative effects (hadronisation corrections).

Both the f_k and the $\hat{\sigma}_{i,k}$ are sensitive to the strong coupling. The partonic cross sections are given in terms of the perturbative expansion in orders of $\alpha_s(\mu_R)$

$$\hat{\sigma}_{i,k} = \sum_n \alpha_s^n(\mu_R) \hat{\sigma}_{i,k}^{(n)}(x,\mu_R,\mu_F) \,. \tag{5}$$

The hard coefficients $\hat{\sigma}_{i,k}^{(n)}$ are calculated for the expansion up to $O(\alpha_s^3)$ taking into account properties of the jet algorithm in the integration over the phase space. The renormalisation scale dependence ('running') of the coupling satisfies the renormalisation group equation

$$\mu_R^2 \frac{d\alpha_s}{d\mu_R^2} = \beta(\alpha_s) \,. \tag{6}$$

The QCD beta-function β is known at 4-loop accuracy. The strength of the coupling thus may be determined at an arbitrary scale, which is conventionally chosen to be the mass of the Z-boson.

The PDFs f_k exhibit a dependence on $\alpha_s(m_Z)$, which can be schematically expressed as

$$\mu_F^2 \frac{df}{d\mu_F^2} = \mathcal{P}(\alpha_s) \otimes f \tag{7}$$

with $\mathcal{P}$ being the QCD splitting kernels and the symbol '⊗' denoting a convolution. After fixing the x-dependence of the PDFs f_k at a scale μ_0 and setting $\mu_R = \mu_F$, the PDF at any factorisation scale μ_F is calculated as

$$f(x,\mu_F,\alpha_s(m_Z)) = \Gamma(\mu_F,\mu_0,\alpha_s(m_Z)) \otimes f_{\mu_0}(x) \tag{8}$$

with Γ being the evolution kernel which obeys equation 7. It is here calculated in NNLO, i.e. in 3-loop accuracy [13, 14], with five active flavours.

The evolution starting scale is chosen to be $\mu_0 = 20\,\text{GeV}$. The PDFs at $\mu_0 = 20\,\text{GeV}$ are provided by the NNPDF3.1 PDF set [15] which was obtained with a nominal value of $\alpha_s^{\text{PDF}}(m_Z) = 0.118$.

3.1 The α_s-fit of the jet data

The value of the strong coupling constant is determined in a fit of theory predictions to H1 jet cross sections with a single free fit parameter. The goodness-of-fit quantity, which is subject to the minimisation algorithm, is defined as

$$\chi^2 = \sum_i \sum_j (\log \varsigma_i - \log \sigma_i)\,(V_{\text{exp}} + V_{\text{had}} + V_{\text{PDF}})^{-1}_{ij} \left(\log \varsigma_j - \log \sigma_j\right), \tag{9}$$

where ς_i are the measurements and σ_i the predictions. The covariance matrices express the relative uncertainties of the data (V_{exp}), hadronisation correction factors (V_{had}) and the PDFs (V_{PDF}). The underlying statistical model is that the logarithm of each measurement is normal-distributed within its relative uncertainty. Correlations of the uncertainties among the different data sets and running periods are taken into account. The hadronisation corrections and their uncertainties have been provided together with the jet cross section measurements. The PDF uncertainties are related to the respective PDF set.

In order to study the size of the uncertainties as a function of $\tilde{\mu}$, the fits to inclusive jet and to dijet cross sections are performed using data points exceeding a given value $\tilde{\mu}_{\text{cut}}$. The resulting uncertainties are displayed in figure 4 (left). The experimental uncertainties are smaller for lower $\tilde{\mu}$ because more data are considered in the fit. In contrast, the scale uncertainties of the NNLO cross section predictions are decreasing with increasing $\tilde{\mu}$. For $\tilde{\mu} > 28\,\text{GeV}$ the experimental and scale uncertainties are getting rather similar in size.

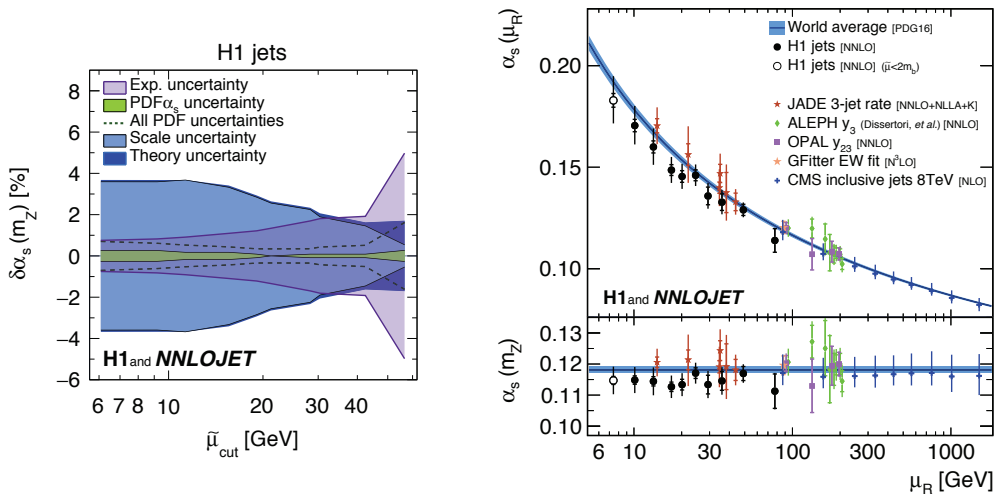

Figure 4. Left: Uncertainties of the α_s fit as a function of $\tilde{\mu}_{\text{cut}}$. Right: Results for $\alpha_s(\mu_R)$ and $\alpha_s(m_Z)$ for fits to data points arranged in groups of similar μ_R, compared to results from other experiments.

Results for the strong coupling

Running of the strong coupling as a function of the scale μ_R is tested performing fits to the H1 jet data points grouped into intervals of $\tilde{\mu}$ as it is indicated in figure 3. The α_s-fit results are shown in figure 4 (right). The measured $\alpha_s(\mu_R)$ values demonstrate expected running of the strong coupling in the accessible range of approximately 7 to 90 GeV. The results are consistent with other determinations of α_s at NNLO accuracy [16–19] and at NLO at very high scale [20], which are also shown. The values of $\alpha_s(m_Z)$ obtained from the fits are displayed in the bottom panel of figure 4 (right) and good agreement between theory and data is found.

The $\alpha_s(m_Z)$ values obtained in the fits to the individual H1 inclusive jet and dijet data sets are shown in figure 5 (left). They are all found to be consistent. The χ^2/n_{dof} values of the fits are around unity indicating consistency of the individual data sets.

The value of $\alpha_s(m_Z)$ from 'H1 inclusive jets' and from 'H1 dijets' are also shown in figure 5 (left). They have a significantly reduced experimental uncertainty compared to the results for the individual data sets. The fit to H1 jets yields $\chi^2/n_{dof} = 0.98$ for 200 data points and $\alpha_s(m_Z) = 0.1143\,(9)_{exp}\,(43)_{th}$. The $\alpha_s(m_Z)$ value obtained from H1 jet data restricted to $\tilde{\mu} > 28$ GeV is

$$\alpha_s(m_Z) = 0.1157\,(20)_{exp}\,(6)_{had}\,(3)_{PDF}\,(2)_{PDF\alpha_s}\,(3)_{PDFset}\,(27)_{scale}$$

with $\chi^2 = 63.2$ for 91 data points. Although the reduced number of data points leads to an increased experimental uncertainty, the scale uncertainty is found to be reduced significantly and all PDF related uncertainties essentially vanish. Therefore, this $\alpha_s(m_Z)$ determination is taken as the main result. This result as well as the results obtained from the inclusive jet and dijet data separately are consistent with the world average [21].

3.2 Simultaneous α_s and PDF determination

In a complementary approach denoted as 'PDF+α_s-fit' in [2], a fit in NNLO accuracy is performed to determine $\alpha_s(m_Z)$ together with the non-perturbative PDFs. As input to the fit the H1 normalised inclusive jet and dijet cross sections are taken as well as the H1 polarised and unpolarised inclusive NC and charged current (CC) DIS cross section data sample identical to the one used in the H1PDF2012 PDF fit [22].

The PDFs are parametrised at a low starting scale μ_0 which is below the charm-quark mass. Heavy-quark PDFs are generated dynamically and only light-quark PDFs and the gluon distribution have to be determined in the fit. The predictions for the inclusive DIS cross sections are calculated using structure function calculations in NNLO using the zero-mass variable flavour number scheme. For inclusive DIS predictions the scales μ_R^2 and μ_F^2 are set to Q^2 and for jet predictions to $Q^2 + P_T^2$.

For the PDF+α_s-fit all data are restricted to the range $Q^2 > 10\,\text{GeV}^2$ and for jet cross sections $\tilde{\mu}$ above two masses of the b-quark is required in addition. At the starting scale $\mu_0^2 = 1.9\,\text{GeV}^2$ the following functional form is used for description of the parton densities in the proton

$$xf(x)|_{\mu_0} = f_A x^{f_B}(1-x)^{f_C}(1 + f_D x + f_E x^2), \tag{10}$$

where f is one of g, $\tilde{u}$, $\tilde{d}$, $\bar{U}$, $\bar{D}$, denoting the density of the gluon, up-valence, down-valence, up-sea, down-sea, respectively. The strange sea is set to $\bar{s}(x) = f_s \bar{D}$, where $f_s = 0.4$. Parameters f_D and f_E are set to zero by default, but are added for specific flavours in order to improve the fit. The parameters g_A, $\tilde{u}_A$ and $\tilde{d}_A$ are constrained by sum rules. The parameter $\bar{U}_A$ is set equal to $\bar{D}_A(1 - f_s)$. The parameter $\bar{U}_B$ is set equal to $\bar{D}_B$. A total of 12 fit parameters are used to describe the PDFs.

The uncertainty obtained from the fit comprises experimental uncertainties of the data and hadronisation uncertainties of the jet cross section predictions. The resulting uncertainty of $\alpha_s(m_Z)$ from the

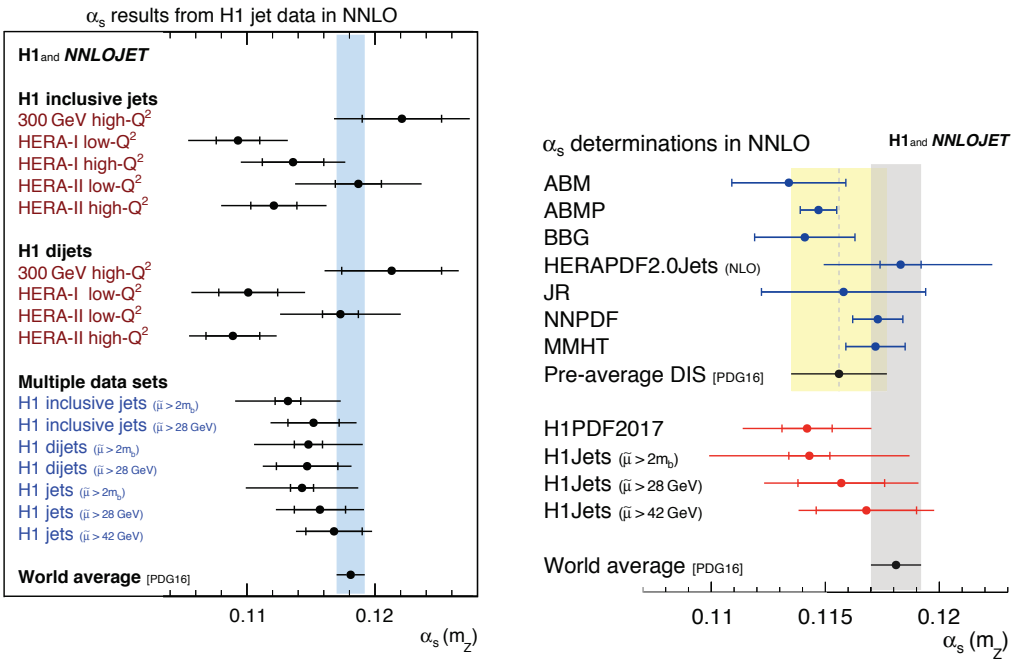

Figure 5. Summary of $\alpha_s(m_Z)$ values obtained in the α_s-fits to individual and multiple H1 jet data sets and in the H1PDF2017 [NNLO] PDF+α_s-fit. The inner error bar indicate the experimental uncertainty and the outer error bars the total uncertainty. The results are compared to the world average and (right figure) to other NNLO α_s determinations from DIS data.

PDF+α_s-fit is denoted as 'exp,had,PDF'. The model uncertainty ('mod') is estimated as the quadratic sum of the differences of the nominal result to the resulting values of α_s when repeating the fit with alternative values of the input parameters. Parametrisation uncertainties ('par') are attributed by adding extra f_D or f_E parameters to the fit or by varying the starting scale or by addition of a more flexible functional form for the gluon, similar to the PDF parametrisation used for the HERAPDF2.0 [23] fit. In total eight parametric forms different from the default are considered. The scale uncertainty of $\alpha_s(m_Z)$ is determined by repeating fits with scale factors 0.5 and 2 applied to μ_R and μ_F simultaneously to all calculations involved.

The PDF+α_s-fit differs from the α_s-fit in the following aspects: the usage of normalised jet cross sections, the inclusion of NC and CC DIS cross sections and the low starting scale μ_0 of the DGLAP evolution, thus assuming the validity of the running coupling and the PDF evolution down to lower scale values.

Fit results and the value of $\alpha_s(m_Z)$

The fit yields $\chi^2/n_{\text{dof}} = 1539.7/(1529 - 13)$, confirming good agreement between the predictions and the data. The resulting PDFs are able to describe 141 jet data points and the inclusive DIS data

simultaneously. The value of $\alpha_s(m_Z)$ is determined to be

$$\alpha_s(m_Z) = 0.1142\,(11)_{\mathrm{exp,had,PDF}}\,(2)_{\mathrm{mod}}\,(2)_{\mathrm{par}}\,(26)_{\mathrm{scale}}\,.$$

This value is consistent with the results of the α_s-fits shown in figure 5, and with the world average. The $\alpha_s(m_Z)$ result is also compared in figure 5 (right) to values from the PDF fitting groups ABM [24], ABMP [25], BBG [26], HERAPDF [23], JR [27], NNPDF [28] and MMHT [29]. and consistency is found. The result is consistent with other determinations and has a competitive experimental uncertainty.

PDF parametrisation results

The PDF and $\alpha_s(m_Z)$ parameters determined together in the PDF+α_s-fit are denoted as H1PDF2017 [NNLO], which is available in the LHAPDF [30] format with experimental, hadronisation and $\alpha_s(m_Z)$ uncertainties included. The gluon and singlet momentum distributions, xg and $x\Sigma$, the latter defined as the sum of all quark and anti-quark densities, are compared to NNPDF3.1 at a scale $\mu_F = 20\,\mathrm{GeV}$ in figure 6 (left) and their ratios to NNPDF3.1 are shown in figure 6 (middle). Within uncertainties, the gluon and singlet distributions obtained for H1PDF2017 [NNLO] are in fair agreement with NNPDF3.1. Note that there are differences in the datasets used for the fits. For H1PDF2017 [NNLO] only H1 data are considered, restricted to the range $Q^2 > 10\,\mathrm{GeV}^2$. For NNPDF3.1 the combined HERA DIS data [23] are used, starting from $Q^2 > 3.5\,\mathrm{GeV}^2$. Data from other processes and experiments are also included, but no DIS jet data.

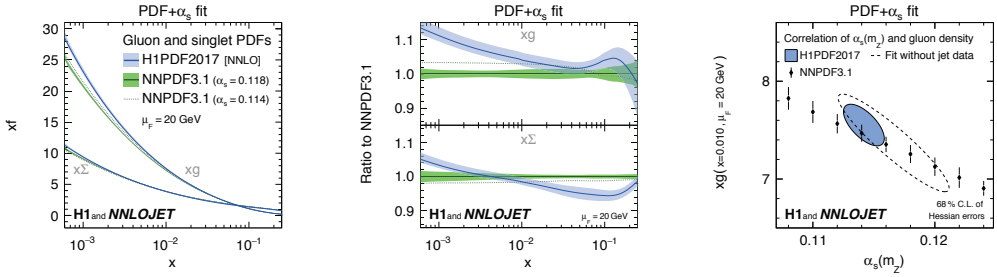

Figure 6. Left: Gluon and singlet distributions at $\mu_F = 20\,\mathrm{GeV}$ determined in the H1PDF2017 [NNLO] PDF+α_s-fit, as a function of the convolution variable x. The PDFs are compared to the NNPDF3.1 PDFs determined with values of $\alpha_s^{\mathrm{PDF}}(m_Z)$ of 0.114 and 0.118. Middle: Ratios of distributions to NNPDF3.1. Right: Error ellipses of Hessian uncertainties at 68 % confidence level of $\alpha_s(m_Z)$ and the gluon density xg at $\mu_F = 20\,\mathrm{GeV}$ and $x = 0.01$ as a result of two different PDF+α_s-fits. The filled ellipse indicates the result of the H1PDF2017 [NNLO] fit and the dashed line of a PDF+α_s-fit with jet data excluded.

The impact of H1 jet data on PDF fits

The PDF+α_s-fit is repeated with the normalised jet data excluded, i.e. only inclusive DIS data are considered. For this fit and the H1PDF2017 [NNLO] fit the gluon distribution $xg(x, \mu_F)$ is evaluated at $\mu_F = 20\,\mathrm{GeV}$ and $x = 0.01$ and its Hessian uncertainty together with its correlation coefficient with $\alpha_s(m_Z)$ are calculated. The resulting Hessian error ellipses are displayed in figure 6 (right) at a

confidence level of 68 %. Compared to the fit without jet data, the inclusion of jet data significantly reduces the uncertainties of $\alpha_s(m_Z)$ and xg, as well as their correlation. Also shown is the gluon distribution of NNPDF3.1 determined for different values of $\alpha_s^{\mathrm{PDF}}(m_Z)$. At this particular choice of x and μ_F, the gluon density of H1PDF2017 [NNLO] is found to be consistent with NNPDF3.1 in the range where $\alpha_s^{\mathrm{PDF}}(m_Z)$ is close to the result of the H1PDF2017 [NNLO] fit.

The inclusion of jet data stabilises the gluon density determination and allows for a simultaneous determination of xg and $\alpha_s(m_Z)$, with a precision on xg competitive to global PDF fits obtained using fixed value of $\alpha_s^{\mathrm{PDF}}(m_Z)$.

4 Summary

Measurements of the inclusive jet, dijet and trijet cross sections in NC DIS at HERA in the H1 experiment are accomplished by measurements at low Q^2 in the range $5.5 < Q^2 < 80\,\mathrm{GeV}^2$ and by an extention of inclusive jet measurements at $150 < Q^2 < 15\,000\,\mathrm{GeV}^2$ to low jet transverse momenta of $5 < P_T^{\mathrm{jet}} < 7\,\mathrm{GeV}$. The precision of the measurements is in the range of 6% to 20%, with the exception of the highest P_T^{jet} bins. The jet cross sections normalised to the inclusive NC DIS cross sections are also obtained. The new jet measurements are fairly well described by the QCD calculations at NLO, NNLO and approximate NNLO (aNNLO) corrected for hadronisation effects.

The new NNLO QCD calculations for jet production cross sections in NC DIS are exploited for a determination of the strong coupling constant $\alpha_s(m_Z)$ using inclusive jet and dijet cross section measurements published by the H1 collaboration.

In the first approach H1 inclusive jet and dijet data are analysed. The cross section predictions account for the α_s dependence in the two components of the calculations, the partonic cross sections and the parton distribution functions (PDFs). The strong coupling constant is determined to be $\alpha_s(m_Z) = 0.1157\,(20)_{\mathrm{exp}}\,(29)_{\mathrm{th}}$, where the jet data are restricted to high scales $\tilde{\mu} > 28\,\mathrm{GeV}$. Values of $\alpha_s(m_Z)$ determined from inclusive jet data or dijet data alone are found to be consistent with the main result. All results are found to be consistent with each other and with the world average value of $\alpha_s(m_Z)$. The running of the strong coupling constant is tested in the range of approximately 7 to 90 GeV and found to be consistent with the expectations.

In a second approach a combined determination of PDF parameters and $\alpha_s(m_Z)$ in NNLO accuracy is performed. In this fit all normalised inclusive jet and dijet cross sections published by H1 are analysed together with all inclusive NC and CC DIS cross sections determined by H1. Using the data with $Q^2 > 10\,\mathrm{GeV}^2$, the value of $\alpha_s(m_Z)$ is determined to be $\alpha_s(m_Z) = 0.1142\,(28)_{\mathrm{tot}}$. Consistency with the other results and the world average is found. The resulting PDF set H1PDF2017 [NNLO] is found to be in fair agreement with NNPDF3.1.

This is the first precision extraction of $\alpha_s(m_Z)$ from jet data at NNLO involving a hadron in the initial state. The NNLO calculations improve significantly the description of the data and reduce the dominating theoretical uncertainty on $\alpha_s(m_Z)$ in comparison to previously employed NLO calculations. All jet cross section measurements are found to be well described by the NNLO predictions. These NNLO calculations are employed for a PDF determination for the first time.

References

[1] H1 Collaboration, V. Andreev *et al.*, *Eur. Phys. J.* **C77** (2017) 215 [arXiv:1611.03421].

[2] H1 Collaboration, V. Andreev *et al.*, *Eur. Phys. J.* **C77** (2017) 791 [arXiv:1709.07251].

[3] H1 Collaboration, V. Andreev *et al.*, *Eur. Phys. J.* **C75** (2015) 65, [arXiv:1406.4709].

[4] J. Currie, T. Gehrmann and J. Niehues, *Phys. Rev. Lett.* **117** (2016) 042001 [arXiv:1606.03991].

[5] J. Currie, E. W. N. Glover and J. Pires, *Phys. Rev. Lett.* **118** (2017) 072002 [arXiv:1611.01460].
[6] J. Currie, T. Gehrmann, A. Huss and J. Niehues, *JHEP* **1707** (2017) 018 [arXiv:1703.05977].
[7] J. Currie, A. Gehrmann-De Ridder, T. Gehrmann, E. W. N. Glover, A. Huss and J. Pires [arXiv:1705.10271].
[8] S. Schmitt, JINST **7** (2012) T10003 [arXiv:1205.6201].
[9] K. Charchula, G. A. Schuler and H. Spiesberger, *Comp. Phys. Commun.* **81** (1994) 381, DJANGOH V1.4.
[10] H. Jung, *Comp. Phys. Commun.* **86** (1995) 147, RAPGAP V3.1.
[11] T. Biekötter, M. Klasen and G. Kramer, *Phys. Rev.* **D92** (2015) 074037 [arXiv:1508.07153].
[12] T. Biekötter, M. Klasen and G. Kramer, private communication, October 2016.
[13] S. Moch, J. A. M. Vermaseren and A. Vogt, *Nucl. Phys.* **B688** (2004) 101 [arXiv:hep-ph/0403192].
[14] A. Vogt, S. Moch and J. A. M. Vermaseren, *Nucl. Phys.* **B691** (2004) 129 [arXiv:hep-ph/0404111].
[15] The NNPDF Collaboration, R. D. Ball *et al.* [arXiv:1706.00428].
[16] Gfitter Collaboration, M. Baak *et al.*, *Eur. Phys. J.* **C74** (2014) 3046 [arXiv:1407.3792].
[17] OPAL Collaboration, G. Abbiendi *et al.*, *Eur. Phys. J.* **C71** (2011) 1733 [arXiv:1101.1470].
[18] JADE Collaboration, J. Schieck, S. Bethke, S. Kluth, C. Pahl and Z. Trocsanyi, *Eur. Phys. J.* C**73** (2013) 2332 [arXiv:1205.3714].
[19] G. Dissertori, A. Gehrmann-De Ridder, T. Gehrmann, E. W. N. Glover, G. Heinrich and H. Stenzel, *JHEP* **0802** (2008) 040 [arXiv:0712.0327].
[20] CMS Collaboration, V. Khachatryan *et al.*, *JHEP* **1703** (2017) 156 [arXiv:1609.05331].
[21] Particle Data Group Collaboration, C. Patrignani *et al.*, *Chin. Phys.* **C40** (2016) 100001.
[22] H1 Collaboration, F. D. Aaron *et al.*, *JHEP* **1209** (2012) 061 [arXiv:1206.7007].
[23] H1 and ZEUS Collaboration, H. Abramowicz *et al.*, *Eur. Phys. J.* **C75** (2015) 580 [arXiv:1506.06042].
[24] S. Alekhin, J. Blümlein and S. Moch, *Phys. Rev.* **D86** (2012) 054009 [arXiv:1202.2281].
[25] S. Alekhin, J. Blümlein, S. Moch and R. Placakyte [arXiv:1701.05838].
[26] J. Blümlein, H. Böttcher and A. Guffanti, *Nucl. Phys.* **B774** (2007) 182 [arXiv:hep-ph/0607200].
[27] P. Jimenez-Delgado and E. Reya, *Phys. Rev.* **D79** (2009) 074023 [arXiv:0810.4274].
[28] R. D. Ball, V. Bertone, L. Del Debbio, S. Forte, A. Guffanti, J. I. Latorre, S. Lionetti, J. Rojo and M. Ubiali, *Phys. Lett.* **B707** (2012) 66 [arXiv:1110.2483].
[29] L. A. Harland-Lang, A. D. Martin, P. Motylinski and R. S. Thorne, *Eur. Phys. J.* **C75** (2015) 204 [arXiv:1412.3989].
[30] A. Buckley, J. Ferrando, S. Lloyd, K. Nordström, B. Page, M. Rüfenacht, M. Schönherr and G. Watt, *Eur. Phys. J.* **C75** (2015) 132 [arXiv:1412.7420].